Proceedings of the 2009 ASME Summer Heat Transfer Conference
July 19-23, 2009, San Francisco, California, USA

HT2009-88263

SIMULATION OF WHISPERING-GALLERY MODE MICROSENSING IN A MICROFLUIDIC SYSTEM

Lei Huang
Department of Mechanical and Aerospace Engineering, Rutgers University, Piscataway, NJ 08854, USA

Zhixiong Guo
Department of Mechanical and Aerospace Engineering, Rutgers University, Piscataway, NJ 08854, USA
E-Mail: Guo@jove.rutgers.edu

ABSTRACT

Label-free detection using a whispering-gallery model biosensor in a micro fluidic channel is simulated. The analyte transport in the solution is controlled by applied electric potentials and diffusion. The finite element method is employed for solving the charged species transportation equations, the Poisson equation, the equations of conservation of momentum and energy, and the Helmholtz equations for electromagnetic waves. The adsorption process of analyte on the micro resonator surface is monitored by the resonance wavelength shift in the sensor. Shift caused by temperature variation due to Joule heating is found to be negligible compared to that induced by analyte deposition. The deposition induced shifts behave in a manner similar to Langmuir-like adsorption kinetics. A linear correlation between the frequency shift and the analyte concentration in the solution is obtained. The applied voltage is found to affect the adsorption capability; and thus, the sensor sensitivity. Detection of very low concentration to the sub-ppm level using the sensor is demonstrated.

INTRODUCTION

Thanks to the recent advance in optical techniques, many different detection methods have been widely applied in biomedical analyses. These methods can be broadly classified into two main categories: labeling methods and label-free methods. Labels can structurally and functionally interfere with an assay. As a result, scientists and biotechnologists have been exploring the area of label-free detection in order to overcome these disadvantages with label methods. Without the need for labels or agents, detection can be done *in situ* and in real time, which is an important advantage in emerging point-of-care detecting applications.

Several label-free optical techniques have been developed, like autofluorescence [1], confocal Raman spectroscopy [2], optical scattering [3], and surface plasmon resonance [4]. However, biophysical studies are hindered by the bulky and expensive equipment needed, and limited cell and biomolecule manipulation and techniques. Consequently, the micro optical fluidic system (MOFS) [5, 6], which employs optics and micro fluidics in a micro system environment to perform novel functionality and in-depth analysis in the biophysical area, has been highly driven by recent development in biophysical studies. In this work, we briefly present the primary mechanism of a micro optical fluidic system, consisting of a microfluidic channel to manipulate samples and a whispering-gallery mode (WGM) biosensor. We believe that the miniature optical WGM device can be used in MOFS to provide an advantage in label-free detection with high sensitivity in the analysis of bio-molecules or single living cells [7].

It is well known that light can be confined in a micro-resonator which can be a sphere [8], a disc [9], a ring [10], or a torus [11]. At resonance, electromagnetic (EM) waves of a specific wavelength are trapped and internally reflected in an orbit within the resonator surface of circular shape. The so-called WGM resonance induces an evanescent wave field in the surrounding medium and extends up to one wavelength outward. This wave can be explored to detect polarizable molecules binding to the surface of the micro-resonator, which can slightly change the resonance condition through interaction with the evanescent waves [7, 12].

WGM resonance frequencies depend on the size and refractive index of the resonator. As the photon guided by total internal reflection (TIR) in a resonator circulates many times, it interacts repeatedly with the adsorbate on the surface of the resonator, leading to change of effective size or refractive index. This feature is broadly explored for use in WGM-based sensors [13, 14]. In general, the resonant modes are approximately predicted by $2\pi r = mc_0 / (f_m \cdot n)$, where m is an integer representing the possible mode, r is the resonator radius, c_0 is

the light speed in vacuum and n is the refractive index of micro resonator. The wavelength shift of a given resonant mode assuming constant refractive index is estimated as [9]: $-\frac{\Delta f}{f}=\frac{\Delta\lambda}{\lambda}\approx\frac{\Delta r}{r}$, where Δr represents a small change of the radius. If we consider the linewidth of the resonance to be the smallest measurable shift (taken as $\Delta f = 10MHz, \lambda = 800nm$), then the smallest "measurable" size change is $2.6\times10^{-5}\,nm$, with the radius $r \sim 1\mu m$. The "measurable" limit turns out to be less than the size of one atom. On the other hand, the ambient temperature variation or the absorption of laser energy during laser scanning or pumping could cause changes to resonator material properties like thermal expansion and thermo-optic effect, impacting the resonator size and refractive index. In 2008, Ma *et al.* [15] measured optical resonance shifts against temperature changes for different silica beads. The measured sensitivity for beads greater than $200\mu m$ in size closely matches the analytical value based on bulk material properties of silica thermal expansion and the thermo-optic effect.

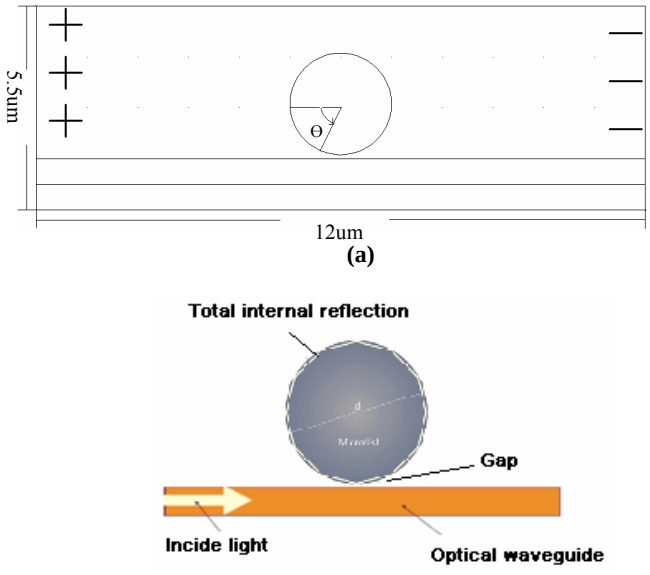

Fig. 1. Sketches of (a) the MOFS and (b) the WGM sensor embedded inside the micro channel of the MOFS.

In what follows, we investigate a model of micro optical fluidic system which combines a micro fluidic channel and WGM-based biosensor to provide a platform for various studies of biophysics, such as molecules detection and bio-molecule analysis. The biosensor is integrated into the MOFS and the microchannel has solution containing the analyte with concentration to be determined by the WGM resonator. The flow is driven by the electric potential applied. The whole process is governed by charge transportation equation, the Poisson equation, the continuity and conservation of momentum equations, the conservation of energy equation and the Maxwell's equations. All governing equations are solved via the finite element method. Emphasis is placed on investigating the optical resonance shifts induced by analyte deposition on the surface.

Table I. Parameters used in this work (Values are taken at 25° C)

Symbol	Description	Value used
w_1	Mobility of BSA in water	$1.6\times10^{-13}\,mol\cdot s/Kg$[16]
$w_i, i=2,3$	Mobility of hydroxide and hydronium ions	$5\times10^{-13}\,mol\cdot s/Kg$[17]
D_1	Diffusivity of BSA in water	$3.91\times10^{-9}\,m^2/s$[18]
$D_i, i=2,3$	Diffusivity of hydroxide and hydrogen ions	$5.3\times10^{-11}\,m^2/s$[19]
K_{ads}	Adsorption coefficient for BSA	$1\times10^{-2}\,m^3/(mol\cdot s)$[20]
K_{des}	Desorption coefficient for BSA	$1\times10^{-5}1/s$[20]
Θ	Surface concentration when the resonator is fully covered by analyte	$10^{-5}\,mol/m^2$
ε	Permittivity for water	$6.93\times10^{-10}\,C/V\cdot m$
σ	Electrical conductivity for Silicon Nitride	$1\times10^{10}\,\Omega\cdot m$
F	Faraday constant	$9.65\times10^{4}\,C/mol$
ρ	Density for water	$10^{3}\,Kg/m^3$
υ	Viscosity for water	$10^{-6}\,m^2/s$
n_s	Refractive index of Silicon Nitride	2.01
n_m	Refractive index of water	1.33
n	Refractive index of BSA	1.5
K_1	Thermal conductivity for Silicon Nitride	$30W/(m\cdot K)$
K_2	Thermal conductivity for water	$0.58W/(m\cdot K)$
c_{p1}	Specific heat capacity for Silicon Nitride	$710.6J/(Kg\cdot K)$
c_{p2}	Specific heat capacity for water	$4.181kJ/(Kg\cdot K)$

MATHEMATIC FORMULATION

Considering a MOFS of planar structure as shown in Fig. 1, the microchannel with analyte solution has a dimension of $12\mu m\times5.5\mu m$. The WGM-based optical resonator coupled with a light-guided waveguide is integrated in the middle of the micro channel. Analytes are directed to the optical resonator through the channel by an electrostatic flow. Fig. 1 (b) provides a more detailed sketch of the optical resonator that is 2 μm in diameter and coupled with a light-delivery waveguide 0.5 μm wide. The gap between the micro resonator and waveguide is defined as 80 nm. A laser beam is focused into the waveguide. Photons at resonant frequencies tunnel from the waveguide to the micro resonator through the small gap and are trapped inside the

resonator by TIRs if the refractive index of the micro resonator is larger than that of the surrounding medium such as water or air. After consecutive TIRs, the resonance occurs if the light wave returns to its starting point in phase.

In our simulation study, we take Bovine Serum Albumin (BSA) with a 2D dimension of $4nm \times 4nm$ [21] as the sample analyte and pure water as solvent to investigate the transport and deposition behaviors. The sample molecular weight and refractive index are assumed as 65325 *g/mol* and 1.5, respectively. Other properties of the working samples, solvent and micro resonator are discussed in what follows and summarized in Table I.

A. Governing equations

We start with the charge transportation equations for analyte samples dissolving in a solution of pure water, including one charged analyte (BSA is taken in this study, appearing a net negative charge in solution with neutral PH [21]), the hydroxide ions and hydronium ions (hydrogen ions bonding to water molecules) [22]:

$$\frac{\partial c_i}{\partial t} + \vec{V} \cdot \nabla c_i = \nabla \cdot (z_i w_i c_i \nabla \Phi) + D_i \nabla^2 c_i , \quad (1)$$

where the subscripts *i*=1,2,3 represent the analyte, hydroxide ion and hydrogen ion, respectively; c_i is the molar concentration; z_i is the valence number (in this work, we assume $z_1 = z_2 = -z_3 = -1$); w_i is the mobility under an external electric field; Φ is the electric potential; D_i is diffusion coefficient for BSA and oppositely charged species, respectively. Typically, in one-dimensional modeling of electrophoresis, charge neutrality is assumed [23, 24]. However, it is only a crude approximation when the electric field is non-uniform. In this work, charge neutrality is not an assumption. As the electric field is irrotational, it may be more conveniently expressed as the Poisson equation:

$$\varepsilon \nabla^2 \Phi = -\rho_E . \quad (2)$$

where

$$\rho_E = F(\sum_i c_i z_i) . \quad (3)$$

Here ρ_E is the total charge density and ε is the permittivity of the fluid and *F* is the Faraday constant. In the Poisson formulation, we assume the permittivity of the liquid is uniform. In such systems, the conductivity field is dominated by charges densities (the charged analyte, hydroxide and hydronium ions) and constant charges' mobility. To complete the system, we also need the continuity and conservation of momentum equations for the liquid:

$$\nabla \cdot \vec{V} = 0 . \quad (4)$$

$$(\frac{\partial \vec{V}}{\partial t} + \vec{V} \cdot \nabla \vec{V}) = -\frac{\nabla P}{P} + \upsilon \nabla^2 \vec{V} - \frac{\rho_E}{\rho} \nabla \Phi . \quad (5)$$

where ρ is the liquid density, $\vec{V}$ is the flow velocity, *P* is the pressure and υ is the liquid viscosity. The electric flux and species conservation are coupled to the mechanics through the electric force in the momentum equation.

It is well known that in an electrolyte microchannel system, the Joule heating induced by the electric field is always a concern. With no exception, in our study, it is necessary to consider the Joule heating:

$$\rho_i c_{pi} \frac{\partial T_i}{\partial t} + \rho_i c_{pi} \vec{V}_i \cdot \nabla T_i = Q_i - \nabla \cdot (-k_i \nabla T_i) . \quad (6)$$

where Q is the heat generated by current flow when a potential difference is applied to an electrolyte solution, and the subscripts $i = 1, 2$ indicate the bulk solution and micro resonator, respectively. Here, T_i's is the temperature distribution; c_{pi}'s is the heat capacity and k_i's is the thermal conductivity.

The micro resonator and waveguide are made of a dielectric material (Silicon nitride in our study), which is assumed to be linear and isotropic. The light wave propagation and photon tunneling in the device can be described by the time-dependent Maxwell equations [25] as following:

$$\nabla \cdot \vec{E} = \frac{\rho_E}{\varepsilon}, \nabla \times \vec{E} = -\mu \frac{\partial \vec{H}}{\partial t} . \quad (7)$$

$$\nabla \cdot \vec{H} = 0, \nabla \times \vec{H} = J + \varepsilon \frac{\partial \vec{E}}{\partial t} . \quad (8)$$

where $\vec{E}$ and $\vec{H}$ are the electric and magnetic field vectors, respectively; for time-harmonic waves, $\vec{E}(r,t) = \vec{E}(r)e^{i\omega t}$ and ω is the angular frequency, the Maxwell equations are then simplified to Helmholtz equations as follows:

$$\nabla^2 \vec{E} + \mu \omega^2 \varepsilon_c \vec{E} = 0 , \quad (9)$$

$$\nabla^2 \vec{H} + \mu \omega^2 \varepsilon_c \vec{H} = 0 . \quad (10)$$

In which the complex permittivity [26] is introduced as:

$$\varepsilon_c = \varepsilon - i(\sigma_i / \omega) , \quad (11)$$

where $\sigma_i, i = 1, 2$ represents the electrical conductivity of environment solution and silicon nitride.

To determine the conductivity of the environment solution:

$$\sigma_1 = F^2(\sum_i c_i w_i z_i^2) . \quad (12)$$

Under WGM resonances, the EM field in a cylindrical micro resonator typically consists of equatorial brilliant rings. The rings are located on the same plane as the waveguide. Moreover, the MOFS with a microdisk/waveguided integrated has a planar structure. So, it is feasible to adopt a two dimensional theoretical model. In the present calculations we consider the in-plane transverse electric (TE) waves, which indicates that the electric field has only a *z*-component and it

propagates in the *x*-*y* plane. As a result, the fields can be written as:

$$\vec{E}(x,y,t) = \vec{E}_z(x,y)\vec{e}_z e^{i\omega t}, \tag{13}$$

$$\vec{H}(x,y,t) = [\vec{H}_x(x,y)\vec{e}_x + \vec{H}_y(x,y)\vec{e}_y]e^{i\omega t}. \tag{14}$$

B. Boundary conditions

In our analysis, we assume constant temperature and analyte concentration at the outlet and inlet of the microchannel. The constant temperature is taken as 300K and the constant concentrations are defined as values of initial conditions. No-slip conditions on the walls and surface of micro resonator are also assumed. Besides that, the following boundary conditions are employed on the walls:

$$\nabla\Phi \cdot \vec{n} = 0, \tag{15}$$

$$\nabla c_i \cdot \vec{n} = 0, \tag{16}$$

$$\vec{V}\cdot\vec{n} = 0, \vec{V}\cdot\vec{t} = 0, \tag{17}$$

$$\vec{n}\times(\vec{E}_1 - \vec{E}_2) = 0, \vec{n}\times(\vec{H}_1 - \vec{H}_2) = 0, \tag{18}$$

where $\vec{t}$ and $\vec{n}$ are the tangential and normal vectors of the wall, respectively. Eqs. (15) and (16) are respectively the condition that the boundary is nonconductive and there is no ion diffusion across the walls. Eq. (17) is the condition that the walls are not penetrative. Eq. (18) demonstrates the natural continuity condition at the system interface and physical boundaries with respect to Maxwell's equations. In this study, special attention should be paid to the surface conditions of the WGM-based micro resonator.

Under the effect of an electric field flow, samples are directed toward the surface of the micro resonator and bind to it. On a hydrophilic solid surface, the electrostatic attraction between a charged surface and an oppositely charged protein molecule is often the major driving force for adsorption from solution onto the solid surface [27]. Thus, with the assumption that there is no surface diffusion on the micro resonator, boundary conditions with respect to c_i are prescribed as follows:

$$\vec{n}\cdot(-D_1\nabla c_1 + c_1\vec{V}) = -K_{ads}c_1(\Theta - c_s) + K_{des}c_s, \tag{19}$$

$$\nabla c_i \cdot \vec{n} = 0, i = 2,3. \tag{20}$$

Here K_{ads} and K_{des} are adsorption coefficient and desorption coefficients, respectively. Θ indicates the surface density when the surface of resonator is fully covered by analyte molecules. The surface density of adsorbate, c_s, is governed by:

$$\frac{\partial c_s}{\partial t} = K_{ads}c_1\Theta - K_{des}c_s. \tag{21}$$

We should be aware of that the adsorption and desorption process only occur on the surface of the micro resonator.

As to the boundaries of the calculation domain for Maxwell's equations, the low-reflecting boundary condition, which indicates that only a small part of the EM wave is reflected and the wave propagates through the boundary almost as if it were not present, is adopted [28]:

$$\vec{e}_z\cdot\vec{n}\times\sqrt{\mu}\vec{H} + \sqrt{\varepsilon}\vec{E}_z = 0. \tag{22}$$

The light source term $\vec{E}_{0z}$, which propagates inwards through the entry of the waveguide, can be treated as an electrically low-reflecting boundary expressed by:

$$\vec{e}_z\cdot\vec{n}\times\sqrt{\mu}\vec{H} + \sqrt{\varepsilon}\vec{E}_z = 2\sqrt{\varepsilon}\vec{E}_{0z}. \tag{23}$$

In the present computations, the light source term is assumed to be uniform and unity at the entry of the waveguide.

RESULTS AND DISCUSSIONS

Versatile numerical approaches including the finite difference time-domain method [29] and the finite element method (FEM) have been employed to solve the above mathematical models. In the current simulation, the commercial COMSOL package (version 3.3) is applied to perform a finite element analysis because the FEM is very flexible in the treatment of irregular configurations such as the circular geometry or the micro resonator. The electro-kinetics, Joule-heating, the Poisson equation and in-plane TE waves application modes of the COMSOL package are employed.

In this study, simulation work is separated into two parts: firstly, charged species transportations, temperature distribution and the adsorption process are simulated in a domain described as in the figure 1. (a) with 20,196 triangle elements. Locally refined meshes are applied to the vicinity around the micro resonator since more attention should be paid to the adsorption on the surface of micro resonator; all coupled modes are solved by a time dependent solver of COMSOL with a 0.1s step size and the relative tolerance is set as 10^{-6}; afterwards, we employ adsorption and temperature distribution results obtained from the first step of simulation work to represent a single adsorption layer and temperature variation which induce changes to the resonance condition of light traveling inside the micro resonator. The simulation domain is shown in figure 1. (b) and meshed by about 350,000 triangle elements. The existence of the thin adsorption layer (in order of Pico meter) brings in extremely small size of meshes in vicinity around the periphery of the micro resonator; hence, more elements are needed to perform the analysis. Simulations are performed in a DELL PC with one 2.2 GHz CPU and 3.0 GB Memory.

The concept of the maximum element size $d_{\max}$ is introduced for the numerically sensitive areas like the periphery of the resonator, the small waveguide and the gap region to ensure the numerical accuracy and sensitivity. The computational error is found to be less than 5%, when the maximum element size is below 1/8 of the wavelength (~782nm in this work) in computationally sensitive regions.

Monolayer formation

Once we apply a constant potential difference to the MOFS, samples are driven to move (the convection is negligible compared to electro migrate) and some of them will be deposited at the resonator surface. The monolayer formation can be monitored by tracking the resonant wavelength shift of a TE mode. Moreover, special attention should be paid to the resonance shift, which is induced by the effect consisting of the deposition process, which slightly changes the effective refractive index and resonator size through the interaction between the adsorbate and light waves.

Table II. Average temperature change (K) of micro resonator with different bulk concentrations for different applied potentials

Concentration (ppm)	Applied Voltage(V)				
	0.5	1	1.5	2	3
0.65325	0.00013	0.00051	0.0012	0.0021	0.0047
1.3065	0.00024	0.00099	0.0022	0.0040	0.0092
2.6130	0.00047	0.0020	0.0051	0.0077	0.018
3.9195	0.00071	0.0029	0.0073	0.012	0.028

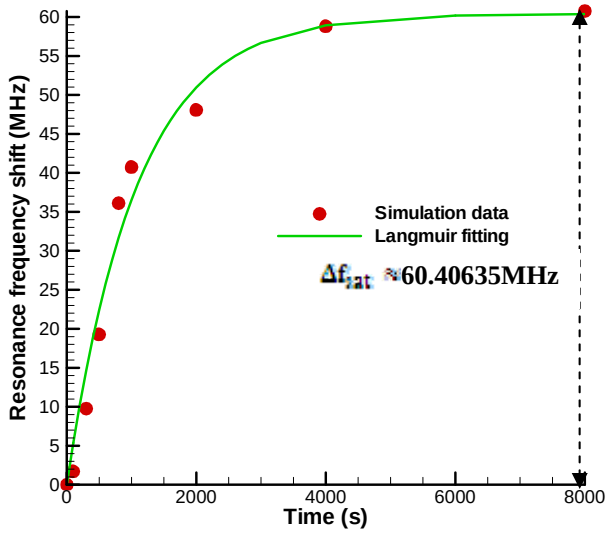

Fig. 2 The time trace of the wavelength shift at 1V applied potential

Ma *et al.* [15] has demonstrated a temperature induced resonance wavelength shifts. Their results match well with the analysis based on bulk material prosperities of thermal expansion and the thermo-optic effect. Analytically, it follows [15]:

$$-\frac{\Delta f}{f}=\frac{\Delta\lambda}{\lambda}=(\alpha+\beta)\Delta T \qquad (24)$$

where α and β are thermal expansion coefficient and thermo-optic effect coefficient, respectively. In this study, the 2D temperature distribution obtained in the thermal simulation has been used to evaluate temperature-dependent refractive indices of the micro resonator and waveguide through a simple relation, $n_{eff}=n_0+(\alpha\Delta T+\beta\Delta T)n$, where n_0 indicates the base refractive index and it is taken as 2.01. Taking the values of $\alpha=1.8\times10^{-6}K^{-1}$ [30] and $\beta=3\times10^{-5}K^{-1}$ [31], the wavelength shift induced by the temperature variation can be obtained. We investigate the average temperature variation from an initial value of 300K of micro resonator with different bulk concentrations for different applied potentials. Results are listed in table II with different average bulk concentrations and applied voltages for each case. All simulation data are obtained with the same conditions except the ones list in table II. By taking temperature change values from table II, the resonance wavelength shifts are in of the range from $10^{-6}\,pm$ to $10^{-4}\,pm$, which is several orders of magnitude lower than the shifts induced by deposition of samples on the surface of micro resonator to be presented later. As a result, the temperature variation induced resonance shifts by means of Joule heating are negligible.

Adsorption of the single layer does not significantly degrade the resonance quality which remains in the range. Figure 2 shows the time evaluation of the frequency down shift induced by the deposition of samples to the surface of micro resonator. The applied potential is set to 1V and the initial concentration of the analyte is assumed to be a uniform distribution of 0.65325 ppm. The time trace of wavelength shifts shows Langmuir-like adsorption kinetics, which points to self-assembly of a single layer formation at saturation. The trace can be fit by a Langmuir-like kinetics, $\Delta f=\Delta f_{sat}(1-e^{-t/\tau})$, where Δf_{sat} is the resonance shift at saturation. Via the best fitting, the time constant is found to be $\tau\approx1077s$ which is very close to the time constant obtained from figure 4, ~1076s. This result provides us the opportunity to monitor the adsorption of analyte onto surface of micro resonator by tracking the detected resonance frequency shifts.

Quan *et al.* [13] showed the sensor curve for measuring and monitoring the growth thickness of peptides. Based on the assumption of the uniformly growth of peptide on the surface of the micro resonator, they found a linear relationship between the peptide thickness and the absolute value of the downshift of resonance frequency, which showed the feasibility of the WGM biosensor as an excellent miniature biosensor in the monitoring of peptide growth and synthesis. However, in our case, the assumption of a uniform distributed analyte on the micro resonator surface is no longer available. Under the effects of an applied electric field, a distribution of the analyte on the micro resonator surface is shown in figure 3 with the starting point referring to figure 1. (a). Different applied voltages with the same initial concentration of 0.65325 ppm are studied. The plot describes the most of the adsorbed analyte distribute in the region where is close to the right surface of micro resonator with respect to Fig. 1. (a). This nonuniform distribution of the adsorbed analyte results from the negatively charged analyte flows toward the anode from an initial normal distribution under the effect of electric field and diffusion . This motion induces a reasonable accumulation of analyte on the right surface of micro resonator which results in a higher surface density in this region.

Assuming constant adsorption and desorption rate, figure 4 demonstrates the average surface density of adsorbed analyte versus different applied potentials. All simulations are performed with a uniform initial concentration of 0.65325 ppm except the applied potential. We observe at steady state, the average thickness of the layer to increase with applied voltage up to 2V. One explanation could be that at the beginning of the adsorption, the process is in the transient transport-limited regime [32], which depends on the bulk analyte concentration in the region of the resonator surface. The higher applied potential results in a bigger velocity of the charged analyte in the region close to surface of micro resonator, hence increases the rate of analyte crossing the region where the adsorption process occurs. Consequently, the analyte at the surface displays a higher concentration.

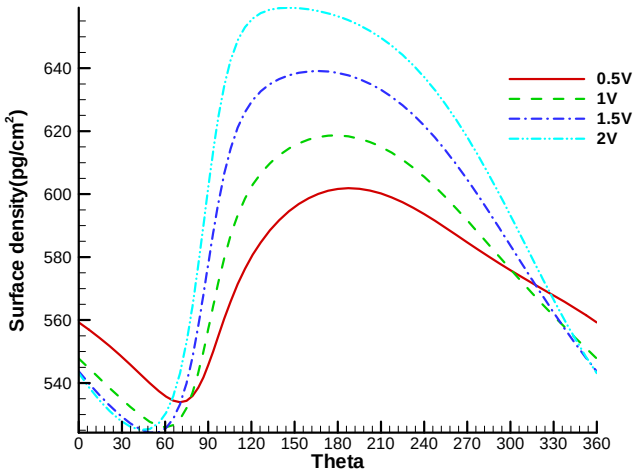

Fig. 3 The surface density distribution of the adsorbed analyte on the micro resonator for different applied potentials

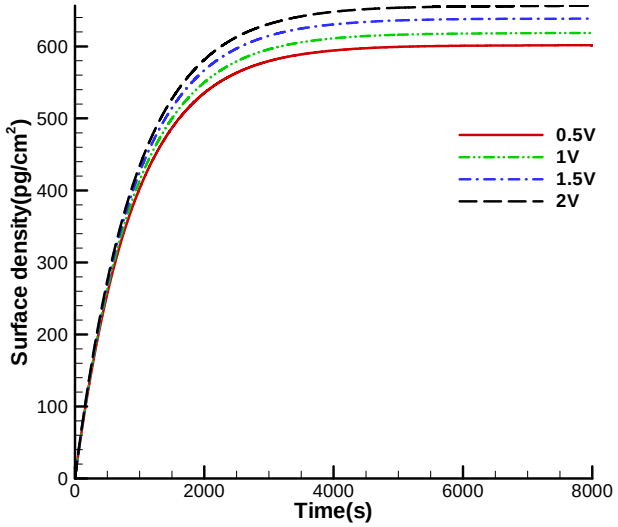

Fig. 4 The time trace of the adsorbed analyte on the surface of micro resonator for different applied potentials

The sample concentration in bulk solution does affect the deposition layer of sample on the surface of micro resonator, which in turn induces a shift to the resonance frequency by slight changes of adsorption layer and refractive index. By tracking of resonance frequency shifts, we are able to investigate the bulk solution conditions. In figure 5, the resonance frequency down-shift curves are plotted for monitoring and measuring the average bulk concentration for different applied potentials. All measurements are performed at steady state. Results show resonance frequency varies with average bulk concentration in an almost linear manner.

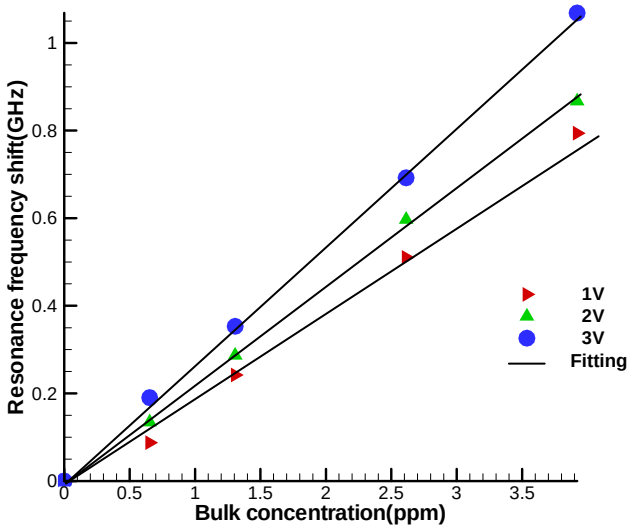

Fig. 5 The resonance frequency shift versus the average bulk concentration for different applied potentials at steady state

Using the best fitting technique, the sensor curve equations are obtained as $\Delta f\,(GHz) = -0.20370 \times c_1$, $\Delta f\,(GHz) = -0.22371 \times c_1$, and $\Delta f\,(GHz) = -0.26858 \times c_1$ for 1V, 2V, and 3V applied potentials, respectively. The correlation coefficients of the linearity are 0.99834, 0.99906, and 0.99868 for 1V, 2V, and 3V applied potentials, respectively. Considering that the linear characteristic is a fundamental requirement for an ideal biosensor, the results show the feasibility of the WGM biosensor as an excellent miniature biosensor in the monitoring of bio-molecules even with a very low concentration. Moreover, the sensor sensitivity increases as the applied voltage increases in the considered voltage range

Conclusions

Integration of WGM and Microfluidics brings a compact manipulating and measuring device. In this MOFS, the analyte was directed to the WGM biosensor through a microchannel flow under the effect of an applied electric field. The whole charged species manipulation and detection processes, including the species transportation in the microchannel, adsorption and desorption processes on the surface of the resonator, the temperature distribution due to Joule heating and the

whispering-gallery mode optical resonances were simulated. Simulations were performed by the finite element analysis based on the COMSOL package. Accurate results are obtained when the appropriate meshes are adopted.

The average temperature changes of micro resonator are obtained at steady state for different bulk concentrations and applied potentials. The change was found to be very small. Hence, the Joule heating induced resonance frequency shift was negligible.

The adsorption process of analyte on the surface of micro resonator can be monitored by tracking the wavelength shift over time. The simulated curve fitted into the Langmuir-like adsorption kinetics well. The WGM sensor was found to function at very low concentrations. Even with a sub-ppm concentration of the charged species, the induced frequency shift is dozens of MHz.

A linear correlation between the average bulk concentration and the resonance frequency shift was obtained. The applied voltage is found to affect the adsorption capability. The analyte density on the sensor surface increases with increasing applied voltage. Therefore, the sensor sensitivity increases as the applied voltage increases in the considered voltage range.

ACKNOWLEDGMENT

This material is based upon work supported by the National Science Foundation under Grant No. CBET-0651737.

REFERENCES

[1] Emmelkamp J, Wolbers F, Andersson H, DaCosta RS, Wilson BC, Vermes I, Berg AVD, 2004, "The potential of auto fluorescence for the detection of single living cells for label-free cell sorting in microfluidic systems," Electrophoresis 25, pp. 3740-3745.

[2] Romano AC, Espana EM, Yoo SH, Budak MT, Wolosin JM, Tseng SCG, 2003, "Different dell sizes in human limbal and central corneal basal epithelia measured by confocal microscopy and flow cytometry," Invest Ophthalmol Vis Sci 44, pp. 5125-5129.

[3] Backman B, Gurjar R, Badizadegan L, Itzkan I, Dasari RR, Perelman LT, Felf MS, 1999, "Polarized light scattering spectroscopy for quantitative measurement of epithelial cellular structures in situ," IEEE J Sel Top Quantum Electron 5, pp. 1019-1026.

[4] Sambles JR, Bradbery GW, Yang FZ, 1991, "Optical-excitation of surface-plasmons - an introduction," Contemp Phys 32, pp. 173-183.

[5] A.Q.Liu, H.J.Huang, L.K.Chin, Y.F.Yu, X.C.Li, 2008, "A review – label-Free detection with micro-optical-fluidic-system (MOFS)," Anal Bioanal Chem 391, pp. 2443-2452.

[6] Guo Z, Maruyama S and Komiya A, 1999, "Rapid yet accurate measurement of mass diffusion coefficients by phase shifting interferometer", J. Phys. D: Appl. Phys., 32, pp. 995-999.

[7] Quan H and Guo Z, 2007, "Simulation of single transpartent molecule interaction with an optical microcavity," Nanotechnology 18, 375702 (5pp).

[8] Gorodetsky M, Savchenkov A, Ilchenko V, "Ultimate Q of optical microsphere resonators," *Opt.Lett.* (1996) **21**, pp. 453-455.

[9] Guo Z, Quan H, and Pau S, 2005, "Optical resonance in fabricated whispering-gallery mode microcavity," J. Heat Transfer, **127** (8), pp. 808-815.

[10] Sumetsky M, Windeler R, Dulashko Y, Fan X, 2007, "Optical liquid ring resonator sensor," Opt. Express 15, pp. 14376-14381.

[11] Ilchenko V, Gorodetsky M, Yao X, Maleki L, 2001, "Microtorus: a high-finesse microcavity with whispering-gallery modes," Opt.Lett. 26, pp. 256-266.

[12] Arnold S, Khoshsima M, Teraoka I, Holler S, Vollmer F, 2003, "Shift of whispering-gallery modes in microspheres by protein adsorption," Opt. Lett. 28, pp. 272-274.

[13] Quan H and Guo Z, 2005, "Simulation of whispering-gallery-mode resonance shifts for optical miniature biosensors," *J.* Quantitative Spectroscopy Radiative Transfer, 93, pp. 231 - 243.

[14] Quan H and Guo Z, 2006 , "Nummerical characterization of whispering-gallery mode optical microcavities," Applied Optics. 45, pp. 611-618.

[15] Ma. Q, Rossmann. T, Guo Z, 2008, "Temperature sensitivity of silica micro-resonators," J. Phys. D: Appl. Phys. 41, 245111 (6pp).

[16] Fumihiro Omasu, Yuta Nakano, Takanori Lchiki, 2005, "Measurement of the electrophoretic mobility of sheep erythrocytes using microcapillary chips," Electrophoresis, 26, pp. 1163-1167.

[17] Crichto. B. H, H. Li, Fouracre . R. A, 1992, "The effect of hydrogen ions in electrolytic solutions on water tree growth in LDPE," IEEE proceeding, pp. 302-305.

[18] *http://www.life.uiuc.edu/crofts/bioph354/diffusion1.html*.

[19] Samson. E, Marchand. J, Snyder. K. A, 2003, "Calculation of ionic diffusion coefficients on the basis of migration test results," Materials and Structures, 36, pp. 156-165.

[20] K. M. Yeung, Z. J. Lu, N. H. Cheung, 2009, "Adsorption of bovine serum albumin on fused silica: Elucidation of protein-protein interactions by single-molecule fluorescence microscopy," Colloids and Surfaces B: Biointerfaces, 69, pp. 246-250.

[21] *http://en.wikipedia.org/wiki/Bovine_serum_albumin*.

[22] H. Lin, Brian D. Storey, Michael H. Oddy, Chuan-Hua Chen, Juan G. Santiago, 2004, "Instability of electrojinetic microchannel flows with conductivity gradients," Phys. Of Fluids 16, pp. 1922-1935.

[23] Gebauer, P., Thormann, W., Bocek, P., 1995, "Sample self-stacking and sample stacking in zone electrophoresis with major sample components of like charge: General model and scheme of possible modes," Electrophoresis 16, pp. 2039-2050.

[24] Jin, Y., Luo, G., 2003, "Numerical calculation of the electroosmotic flow at the cross region in microfluidic chips," Electrophoresis 24, pp. 1242-1252.

[25] Jackson, J. D., "Classical Electrodynamics," 1998, 3rd ed., Wiley, New York.
[26] Modest, M.F., "Radiative heat transfer," 2nd ed., Academic Press, New York.
[27] J R Lu, T J Siu, B J Howlin, R K Thomas, Z F Cui, J Penfold, J R P Webster1998, " Protein-adsorption at interfaces," Scientific highlights, 54-55.
[28] H.Quan, and Z.Guo, 2007, "Energy transfer to optical microcavities with waveguides," J. Heat Transfer 129, pp. 44-52.
[29] Taflove, A., Hagness, S. C., 2005, "Computational electrodynamics: The finite-difference time-domain method,", 3rd ed., Norwood, MA.
[30] *http://accuratus.com/silinit.html*.
[31] R. Amatya, C. W. Holzwarth, H.I. Smith., R. J. Ram, 2007, "Efficient thermal tuning for second-order silicon nitride microring resonators," IEEE., pp. 149-150.
[32] Michelle A. Brusatori, 2003, "Protein adsorption kinetics under an appliedelectricfield: an optical waveguide lightmode An optical waveguide lightmode spectroscopy study," Langumuir,19, pp. 5089-5097.